arXiv:1605.01269v2 [physics.plasm-ph] 18 Sep 2016

Suppression of a laminar kinematic dynamo by a prescribed large-scale shear

Aditi Sood1, **Rainer Hollerbach**2, **Eun-jin Kim**1

1 School of Mathematics & Statistics, University of Sheffield, Sheffield S3 7RH, UK
2 School of Mathematics, University of Leeds, Leeds LS2 9JT, UK

Abstract. We numerically solve the magnetic induction equation in a spherical shell geometry, with a kinematically prescribed axisymmetric flow that consists of a superposition of a small-scale helical flow and a large-scale shear flow. The small-scale flow is chosen to be a local analog of the classical Roberts cells, consisting of strongly helical vortex rolls. The large-scale flow is a shearing motion in either the radial or the latitudinal directions. In the absence of large-scale shear, the small-scale flow operates very effectively as a dynamo, in agreement with previous results. Adding increasingly large shear flows strongly suppresses the dynamo efficiency, indicating that shear is not always a favourable ingredient in dynamo action.

1. Introduction

Many astrophysical objects such as planets or stars possess magnetic fields. The origin of all of these fields is believed to be via so-called dynamo action, whereby the motion of electrically conducting fluid maintains the field against the otherwise inevitable ohmic decay. The full problem involves nonlinearly coupled partial differential equations for the evolution of both the magnetic field and the fluid flow, with each affecting the other. Despite the complexity of this process, numerical solutions have by now progressed to the point where quite detailed and realistic models of different dynamos are routinely being computed [1, 2, 3]. Although dynamos in different astrophysical objects are often very different in many important details, there are nonetheless a few basic ingredients that occur often enough to warrant studying their effects in isolation. Two of these are small-scale helical motions and large-scale shear flows. In this work we will study a kinematically prescribed flow that consists of a superposition of these two. Although simply prescribing the flow, rather than self-consistently solving for it, is of course a simplification of the full problem, this approach has a considerable merit of elucidating the key role of helicity and shear flows and the interaction between different competing effects, which are often difficult to differentiate in a more complete model.

The idea that the helicity, or handedness, of a flow can be a critically important ingredient in dynamo theory is familiar since the so-called mean-field theory was developed in the 1960s (e.g. [4]), in which certain averages are taken, and an α-effect is extracted that is directly proportional to the helicity of the small-scale flow structures. This α-effect can then drive a large-scale dynamo. One particularly simple flow for which the theory can be thoroughly developed is the Roberts flow [5, 6], consisting of a plane-periodic array of helical vortices. A time-periodic version of the Roberts flow [7] has also proven invaluable in studying the distinction between slow and fast dynamos; a necessary condition for fast dynamo action, in which the magnetic field grows on the fast advective timescale rather than the slow diffusive timescale (or any intermediate timescale) is that Lagrangian particle paths be chaotic [8], which in a flow that depends on x and y but not z requires the flow to also depend on t. Another adaptation of a Roberts-type flow was by [9], who fitted a similar array of small-scale cells into a spherical shell. The motivation for this is to introduce a natural largest scale, unlike in plane-periodic geometry, where the largest scale is effectively infinite.

Another ingredient that can play an important role both in dynamo theory generally as well as in particular situations such as the solar tachocline [10], accretion disks [11] or entire galaxies [12] is a large-scale shear. At its most basic, in what is known as the ω-effect, a shear flow can simply take an existing magnetic field and stretch it out, thereby producing a field component along the direction of the shear. A vast number of numerical models [13, 14, 15, 16, 17, 18, 19, 20, 21, 22, 23] include various large-scale shearing motions, and find that it enhances the dynamo efficiency, in flows both with and without helicity. However, numerous other studies [25, 26, 27, 28] find that shear can also be detrimental to dynamo action, for example by disrupting critically important

phase relationships between different small-scale cells. Yet another study [29] finds that shear may enhance large-scale fields but suppress small-scale ones.

It is these conflicting possibilities regarding the effect of a large-scale shear that motivate our work. Specifically, we start with a spherical shell cellular flow similar to that of [9], add to it large-scale shear flows of increasing strength, and consider the dynamo action of these kinematically prescribed flows. By examining the growth rate curves, as functions of magnetic Reynolds number, we show that at least for these small-scale flows, the addition of a large-scale shear always suppresses the dynamo efficiency. We also examine the spatial structures of the resulting eigenmodes, as well as the corresponding magnetic energy spectra, and explore the influence of the shear on these.

2. Governing Equations

In the framework of kinematic dynamo theory, we solve the induction equation

$$\frac{\partial \mathbf{B}}{\partial t} = \nabla \times (\mathbf{U} \times \mathbf{B}) + R_m^{-1} \nabla^2 \mathbf{B} \tag{1}$$

in a spherical shell. The magnetic Reynolds number $R_m = UL/\eta$, where U is a characteristic velocity scale, L a characteristic length scale (taken to be the outer radius of the shell), and η is the magnetic diffusivity of the fluid. The prescribed velocity field $\mathbf{U}$ is axisymmetric, and consists of a super-position of a small-scale helical flow and a large-scale shear flow.

The small-scale flow has the form $\nabla \times (\psi \hat{\mathbf{e}}_\phi) + v \hat{\mathbf{e}}_\phi$, where the meridional circulation ψ and the azimuthal velocity v are given by

$$\psi = \frac{1}{N_\theta} r \sin\left(\frac{(r - r_i)}{(r_0 - r_i)} N_r \pi\right) \sin\theta \cos\theta \cos(N_\theta \theta), \tag{2}$$

$$v = \sin\left(\frac{(r - r_i)}{(r_0 - r_i)} N_r \pi\right) \sin\theta \cos(N_\theta \theta). \tag{3}$$

This flow is very similar to one of the flows considered by [9], and consists of small-scale cells that are local analogs of the classical Roberts flow [5, 6]. The parameters N_r and N_θ specify the number of cells in the r and θ directions, respectively; we will here always take $N_\theta = 4N_r$, which yields cells that are very close to round. Note also that these flows have $O(1)$ magnitude, and hence a turnover time $\sim N_r^{-1}$ for the small cells.

The main difference between this flow and the previously considered [9] flow is the additional factor of $\cos\theta$ in ψ. Without this factor the helicity of the flow would be equatorially symmetric; with it included we see that ψ is anti-symmetric, v is symmetric, and the helicity is then also anti-symmetric. There are two reasons for modifying the flow in this way. First, it is simply of interest to see whether the previous results [9] continue to hold even if the small-scale flow is only strongly helical in each hemisphere separately, but with zero net helicity. Second, taking ψ to be anti-symmetric and v symmetric allows for the familiar separation of $\mathbf{B}$ into dipole and quadrupole symmetries, and is thus numerically convenient.

Turning next to the large-scale shear flow, this is of the form $S\,r\sin\theta\,\Omega$, where the two choices for the angular velocity Ω are

$$\Omega_1 = (r - 0.75), \qquad \Omega_2 = (\cos^2\theta - 0.5). \tag{4}$$

That is, Ω_1 represents a shear purely in the radial direction, whereas Ω_2 represents a shear purely in the latitudinal direction (but still equatorially symmetric, to preserve the dipole/quadrupole decoupling for $\mathbf{B}$). The constants in each case, 0.75 and 0.5, correspond to solid-body rotation, and hence have no effect other than to choose a coordinate system where the average value of Ω is comparatively small. We emphasize also that both the small-scale and the large-scale flows are simply prescribed, rather than being solutions of the Navier-Stokes equation. If $\mathbf{U}$ were evolved according to the Navier-Stokes equation, both components would inevitably be far more complicated, and furthermore each would significantly affect the other. By kinematically prescribing $\mathbf{U}$ we are able to avoid this mutual interdependence, and thereby isolate the effect of increasing shear on the dynamo action of the small-scale flow.

To summarize, we solve Eq. (1) in a spherical shell with radii $r_i = 0.5$ and $r_o = 1$, with the total flow given by

$$\mathbf{U} = \nabla \times (\psi\hat{\mathbf{e}}_\phi) + v\hat{\mathbf{e}}_\phi + S\,r\sin\theta\,\Omega, \tag{5}$$

and ψ, v and Ω as above. Each choice of flow, Flow1 in the presence of radial shear, Ω_1, and Flow2 in the presence of latitudinal shear, Ω_2, is therefore completely specified by the two parameters N_r, measuring the number of cells in the radial direction, and S, measuring the strength of the large-scale shear. (Note incidentally that according to this definition the magnetic Reynolds number R_m is based on the magnitude of the small-scale flow; a 'large-scale flow Reynolds number' would require multiplying R_m by S.)

Because the flow $\mathbf{U}$ is axisymmetric, $\mathbf{B}$ decouples into distinct $\exp(im\phi)$ azimuthal modes, each of which further decouple into dipole and quadrupole equatorial symmetries as noted above. In fact, the two symmetries always behaved very similarly, so only dipole results will be presented in detail here. The further details of the numerical solution are exactly as in [9], see also [30]. Resolutions up to 300 Chebyshev polynomials in r and 400 Legendre functions in θ were used, and were carefully checked to ensure fully resolved solutions. See Table 1 for sample convergence results at different resolutions. Typical time-steps used were $O(10^{-3})$, and all solutions were run sufficiently long to allow the dominant eigenmode to emerge.

3. Results

Figure 1 shows growth rates for the two cell sizes $N_r = 5$ and 10, and shear parameter $S = 0$ (so small-scale cells only) and $S = 3$ for the two shearing options. The $S = 0$ results are exactly as one might expect: for increasing R_m the growth rates first increase, then eventually decrease again, as they must for a slow dynamo (since the flow is independent of time). There is also a smooth progression to higher azimuthal

N_r	S_1	S_2	120×240	140×280	160×320	180×360	200×400
5	7	0	0.848	0.824	0.787	0.770	0.762
5	0	7	0.681	0.604	0.563	0.543	0.530
10	7	0	1.054	1.047	1.042	1.038	1.036
10	0	7	1.293	1.201	1.267	1.228	1.245

Table 1: Growth rates for the $N_r = 5$ and 10 flows, with shear parameter $S = 7$ for either Ω_1 or Ω_2, as indicated. For the five resolutions given, the first quantity is the number of Chebyshev polynomials in r, and the second is the number of Legendre functions in θ. The azimuthal wavenumber $m = 10$ for all four rows; other values of m have similar convergence properties. $R_m = 10^4$ for all results; smaller values typically converged even more quickly.

wavenumbers m being the most dominant modes. These results are broadly similar to the previous results [9], including the feature that $N_r = 10$ has a maximum growth rate significantly greater than $N_r = 5$ does. This is because the turnover time of a small cell decreases with N_r while the effective growth rate should be measured in units of turnover time, rendering the effective growth rate (measured in turnover time units) comparable in $N_r = 5$ and 10 cases. Another conclusion is that flows such as these, with strong helicity in each hemisphere, but zero net helicity, still behave much the same as the previous flows with helicity of the same sign everywhere. Turning next to the $S = 3$ sheared cases, the most significant conclusion is that the growth rates are strongly reduced in every case. Furthermore, $N_r = 5$ curves are far less smooth than they were for $S = 0$. This seems to indicate transitions between different eigenmodes due to shear flow – for $S = 0$ the dominant eigenmode always remains the same mode, and just gradually evolves as R_m is increased. The $N_r = 10$ curves also exhibit this mode switching to a certain degree, but considerably less.

Specifically, in addition to the overall reduction in the growth rate, we see a non-monotonic dependence of the growth rate on R_m, accompanied by the shift of the location for the maximum growth rate and/or by the appearance of peaks for secondary maxima. This irregular behaviour is more pronounced in the case of $N_r = 5$ than $N_r = 10$. In order to understand this, it is useful to recall that a large-scale shear flow accelerates the formation of small scales by distorting small scale structures, thereby facilitating the dissipation of small scales by ohmic diffusion [31, 26].

Quantitatively, the effective dissipation rate of small scales is given by the decorrelation rate $1/\tau_\Delta$, by weighting the ohmic dissipation rate $\gamma_\eta = k^2/R_m$ for the mode with wavenumber k by shear strength S_* as follows [31]. That is, in the absence of a shear flow, the dissipation rate of a mode with wavenumber k is given by $\gamma_\eta = k^2/R_m$. In the presence of a shear flow with an effective shear parameter S_*, the dissipation rate of a k mode is faster than γ_η for sufficiently large S_* as a shear flow accelerates the formation of small scales which are then dissipated by Ohmic diffusion. This faster

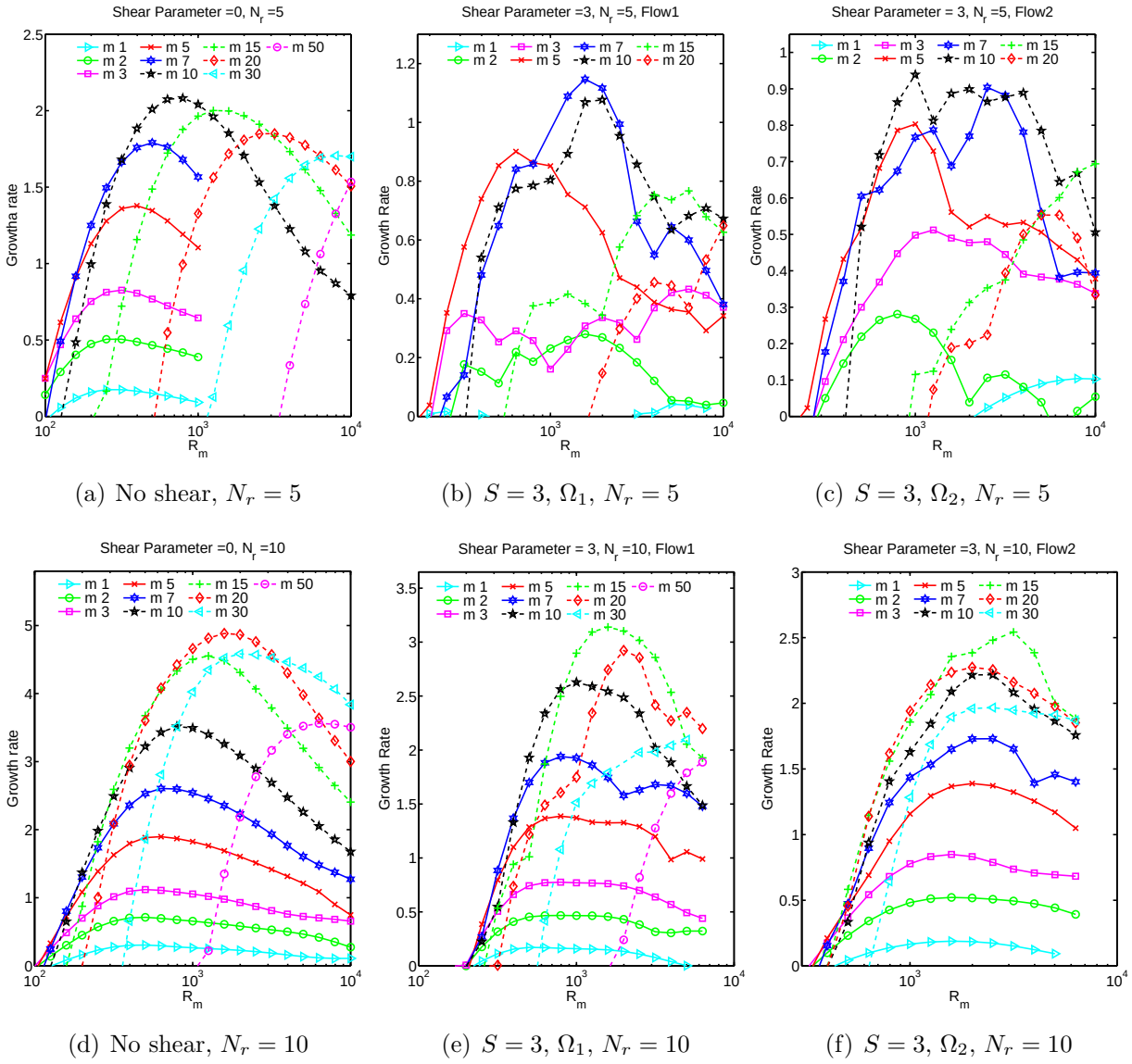

(a) No shear, $N_r = 5$ (b) $S = 3$, Ω_1, $N_r = 5$ (c) $S = 3$, Ω_2, $N_r = 5$

(d) No shear, $N_r = 10$ (e) $S = 3$, Ω_1, $N_r = 10$ (f) $S = 3$, Ω_2, $N_r = 10$

Figure 1: Growth rate curves as functions of R_m. The top row has $N_r = 5$, the bottom row $N_r = 10$. In each row the first panel has $S = 0$, so no large-scale shear at all, the second panel has the shear Ω_1, and the third panel has the shear Ω_2, each with amplitude $S = 3$.

dissipation rate is estimated by the decorrelation rate τ_Δ^{-1} given by

$$\tau_\Delta^{-1} = [\gamma_\eta \, S_*^2]^{1/3} = [\frac{k^2}{R_m} S_*^2]^{1/3}. \tag{6}$$

In Eq. (6), S_* is the effective shear measured in the unit of the characteristic time of small-scale cells

$$S_* = S/N_r,$$

and k is the wavenumber $k \sim m/0.75$ (by using the mean radius of the shells). In the limit of strong shear $S_* > k^2/R_m$, the shear-weighted decorrelation rate is much larger

than the ohmic dissipation rate, leading to the effectively *smaller* Reynolds number R_m^*, defined by the following equality

$$\frac{k^2}{R_m^*} = \left[\frac{k^2}{R_m}\frac{S^2}{N_r^2}\right]^{1/3}, \tag{7}$$

or, alternatively

$$R_m = \left(\frac{R_m^*}{k}\right)^3 \frac{S^2}{kN_r^2}. \tag{8}$$

Therefore, the R_m, which gives the same amount of the ohmic dissipation for R_m when $S = 0$, increases with the shear strength $R_m > R_m^*$. Although the flow and magnetic structures are far more complicated in our model (e.g. compared to the Cartesian model [28]), it is useful to examine the consequence of Eq. (8) by an order of estimate. For instance, for $m = 7$ and $N_r = 5$ for which the maximum growth rate appears around $R_m^* \sim 500$ without shear $S = 0$ in Fig. 1(a), we can estimate the value of R_m when $S = 3$ from Eq. (8) by taking $k \sim 10$ as

$$R_m \sim 4500, \tag{9}$$

offering a possible explanation for the secondary local maximum growth around $R_m \sim 4500$ in Fig. 1(b).

On the other hand, the dominant peak around $R_m \sim 2000$ seems to occur since the growth rate measured in units of turnover time becomes comparable to the decorrelation rate as

$$\frac{\gamma}{N_r} \sim \left[\frac{k^2}{R_m}\frac{S^2}{N_r^2}\right]^{1/3}, \tag{10}$$

Solving Eq. (10) gives R_m as

$$R_m \sim \frac{k^2 N_r S^2}{\gamma^3}. \tag{11}$$

For instance, for the $m = 7$ ($k \sim 10$) mode discussed above, taking $\gamma \sim 1.2$ and $S = 3$, Eq. (11) yields $R_m \sim 2000$.

A key criterion for the quenching of dynamo by a shear flow is whether the effective shear parameter S_* is larger or smaller than the Ohmic dissipation rate $\gamma_\eta = k^2/Rm$ for a mode with wavenumber k. Thus, other competing effects are likely to promote a dynamo for small $S_* < \gamma_\eta$ while in the opposite limit $S_* > \gamma_\eta$, a shear flow could inhibit a dynamo, dominating over other effects.

Compared to $N_r = 5$ case, the effective shear $S_* = S/N_r$ is smaller for $N_r = 10$, with much less effect of shear, and thus much smoother behaviour in the growth rates in Figs. 1(d)-(e). Therefore, for even greater N_r, and hence greater degree of separation between the small-scale and large-scale flows, that the effect of shear is further reduced, curves eventually looking just as smooth as in the $S = 0$ case. Further increasing N_r would unfortunately require prohibitively large numerical resolutions.

Figure 2 quantifies the suppression of the growth rates by increasingly large shear in the two cases. Detailed results are presented here only for the particular value

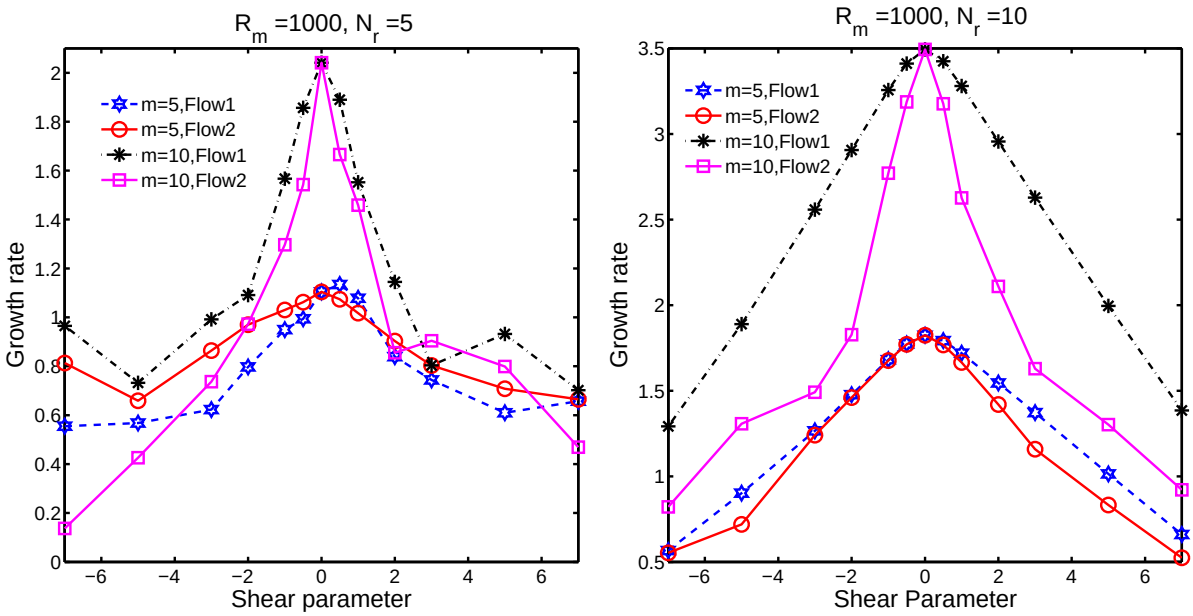

(a) (b)

Figure 2: Growth rates as functions of shear parameter S, indicating the suppression of dynamo action for non-zero S. The left and right panels have $N_r = 5$ and 10, respectively. **Flow1 in the presence of purely radial shear Ω_1, Flow2 in the presence of purely latitudinal shear** Ω_2, and azimuthal wavenumbers $m = 5$ and 10 as indicated, and $R_m = 1000$ throughout.

$R_m = 1000$, close to the peaks in Fig. 1. Other values of R_m behaved qualitatively the same. Similarly, only the two azimuthal wavenumbers $m = 5$ and 10 are presented, but others were also examined and behaved similarly. The overall conclusion is again very clear; even moderate values of S immediately begin to suppress the growth rates, almost in a power law. As observed in Fig. 1, Fig. 2 also exhibits a narrow region of S with local maximum growth rate where the magnetic field is favourable to the growth despite the overall growth inhibition. This seems to be caused by resonance when the characteristic time scale ($1/\omega = 1/N_r$) of the small-scale cells matches the local advection time for mode k due to the shear flow across the cell [28] as

$$N_r \sim kU_* = S(0.5/N_r), \tag{12}$$

where the local mean flow across one single small cell is estimated as $U_* = S(0.5/N_r)$ as there are N_r cells between $r = [0.5, 1]$. Note that Eq. (12) holds when the Doppler-shift frequency vanishes ($\omega - kU_* = 0$). For instance, solving Eq. (12) for S for the case $N_r = 5$ and $m = 10$ ($k \sim 15$), we obtain $S = 3 \sim 5$, explaining the peak in Fig. 2(a). As is clear from Eq. (12), the shear strength S required for the resonance increases quadratically with N_r, occurring for much larger $S > 10$ for $N_r = 10$. This is why Fig. 2(b) shows only the monotonic decrease in the growth rate with increasing $|S|$.

It is interesting also to note that positive and negative values of S yield similar

results, but not identical. This indicates that even for $N_r = 10$ the cells are not so small yet that the dynamo action of the overall pattern does not sense a distinction between the inner and outer edges of the shell (for Flow 1), or between more polar and more equatorial latitudes (for Flow 2)

Figure 3 shows examples of the spatial structure of the resulting eigenmodes. As

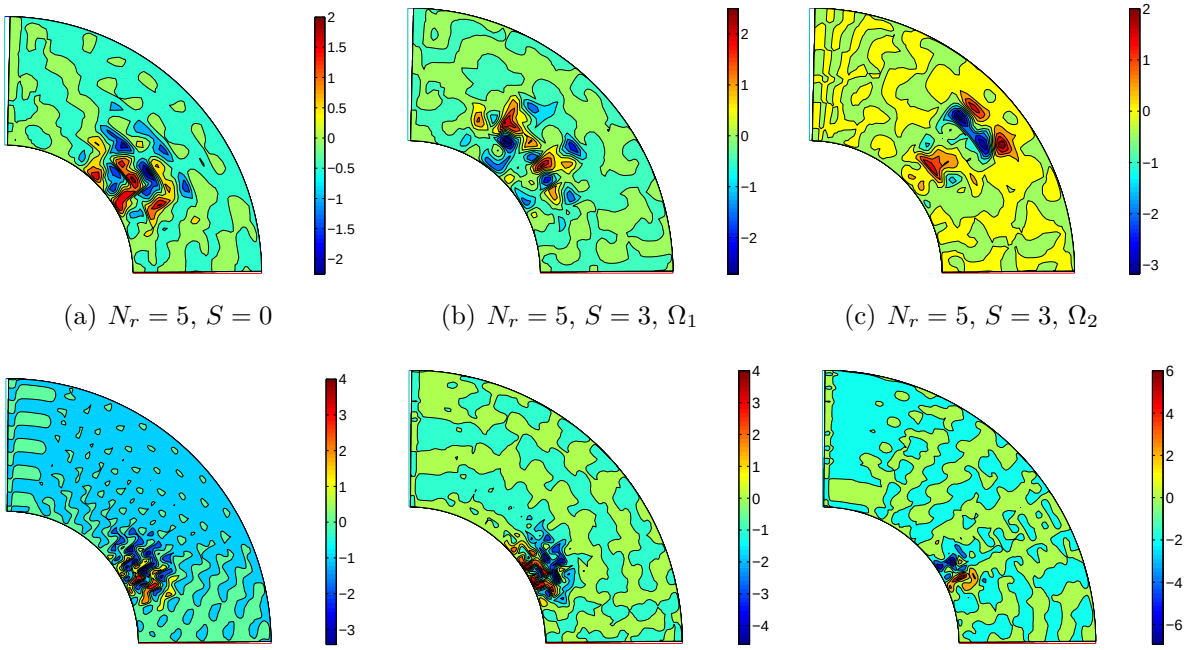

(a) $N_r = 5$, $S = 0$ (b) $N_r = 5$, $S = 3$, Ω_1 (c) $N_r = 5$, $S = 3$, Ω_2

(d) $N_r = 10$, $S = 0$ (e) $N_r = 10$, $S = 3$, Ω_1 (f) $N_r = 10$, $S = 3$, Ω_2

Figure 3: Meridional sections of B_ϕ for $N_r = 5$ (top row) and $N_r = 10$ (bottom row). From left to right $S = 0$ (so either Ω_1 or Ω_2), then Ω_1 and Ω_2, respectively, at $S = 3$. $R_m = 1000$ and $m = 10$ in all cases. The difference between $N_r = 5$ and 10 is clearly visible in terms of the different size structures, but the differences between $S = 0$ and 3 are surprisingly little, given how strongly suppressed the growth rates already are.

expected, the field is organized into structures on the scale of the small-scale cells, and is also strongest at the mid-latitudes where the helicity is strongest. Considering how strongly the growth rates vary, the spatial structures vary surprisingly little.

Finally, Fig. 4 shows the energy spectra of these solutions in Fig. 3, as well as other values of S. Here we can see one clear difference between the two flows. Flow 1, with the purely radial shear, exhibits strong peaks at spherical harmonics l that are multiples of N_θ (recall $N_\theta = 20$ and 40 for $N_r = 5$ and 10, respectively), reflecting the number of small-scale cells. In contrast, for Flow 2 with its latitudinal shear, these peaks have been largely smoothed out, and one obtains much more uniform spectra. Another feature that is particularly noticeable for $N_r = 5$ is that increasing shear causes the spectra to drop off less rapidly; that is, shear promotes small-scale in the magnetic field, in agreement with [31, 26].

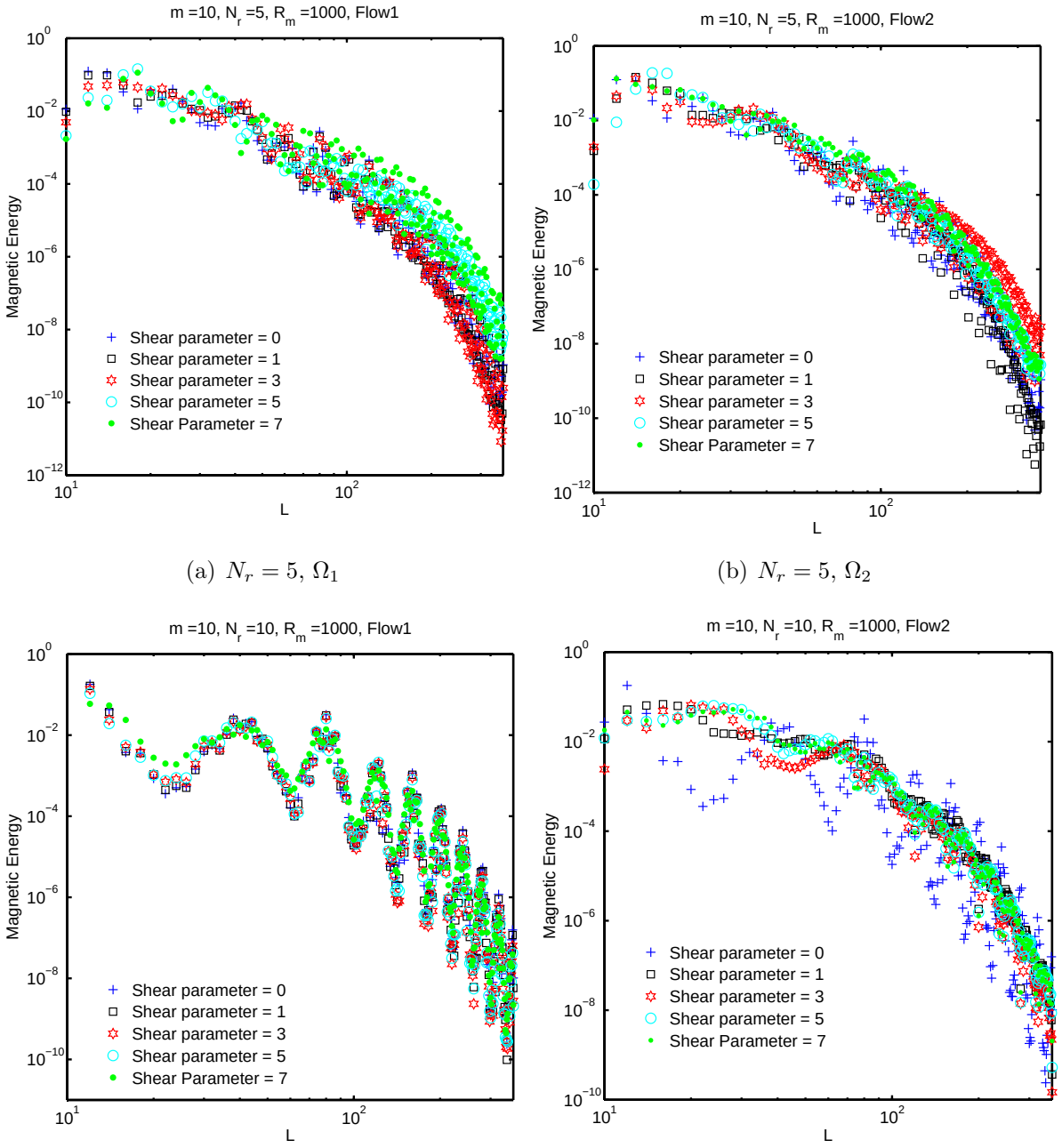
m =10, N_r =5, R_m =1000, Flow1
m =10, N_r =5, R_m =1000, Flow2
m =10, N_r =10, R_m =1000, Flow1
m =10, N_r =10, R_m =1000, Flow2
Magnetic Energy
L
Shear parameter = 0
Shear parameter = 1
Shear parameter = 3
Shear parameter = 5
Shear Parameter = 7

(a) $N_r = 5$, Ω_1 (b) $N_r = 5$, Ω_2

(c) $N_r = 10$, Ω_1 (d) $N_r = 10$, Ω_2

Figure 4: Energy spectra for magnetic field in the presence of shear Ω_1 and Ω_2 at $N_r = 5$ and 10, and $S = 0, 1, 3, 5, 7$ as indicated.

4. Conclusion

We have seen in this work that at least for the small-scale flows considered here, the addition of a large-scale shear always suppresses the dynamo efficiency. There is thus no regime where the direct ω-effect dominates over the more indirect disrupting influences of the shear. One important further direction for future work will be to take the small-

scale flows to be time-dependent, either periodic as in the [7] plane-layer model, or stochastic as in a variety of analytic models [25, 26, 27], and see whether a large-scale shear still always has a negative influence. Time-dependent flows will necessarily involve additional correlation times and phase relationships, and may thus yield different results for at least some parameter combinations.

Another possible extension would be to consider the nonlinear equilibration of these dynamos, which would however require reintroducing the dynamics of $\mathbf{U}$, and hence involve considerable complications over the problem considered here. It is known (e.g. [32]) that dynamically equilibrated magnetic fields can be quite different from the kinematic eigenfunctions, so potentially very rich additional dynamics could emerge.

References

[1] Jones C A 2011 *Ann. Rev. Fluid Mech.* **43** 583
[2] Brandenburg A, Sokoloff D and Subramanian K 2012 *Space Sci. Rev.* **169** 123
[3] Ferrario L, Melatos A and Zrake J 2015 *Space Sci. Rev.* **191** 77
[4] Moffatt H K 1978 *Magnetic Field Generation in Electrically Conducting Fluids* (Cambridge University Press)
[5] Roberts G O 1970 *Phil. Trans. R. Soc. London* A **266** 545
[6] Roberts G O 1972 *Phil. Trans. R. Soc. London* A **271** 411
[7] Galloway D J and Proctor M R E 1992 *Nature* **356** 691
[8] Childress S and Gilbert A D 1995 *Stretch, twist, fold: the fast dynamo* (Berlin: Springer)
[9] Richardson K J, Hollerbach R and Proctor M R E 2012 *Phys. Fluids* **24** 107103
[10] Miesch M S 2005 *Living Rev. Solar Phys.* **2** 1
[11] Balbus S A and Hawley J F 1998 *Rev. Mod. Phys.* **70** 1
[12] Kulsrud R M and Zweibel E G 2008 *Rep. Prog. Phys.* **71** 046901
[13] Rogachevskii I and Kleeorin N 2003 *Phys. Rev. E* **68** 036301
[14] Rogachevskii I and Kleeorin N 2004 *Phys. Rev. E* **70** 046310
[15] Brandenburg A, Rädler K-H, Rheinhardt M and Käpylä P J 2008 *Astrophys. J.* **676** 740
[16] Käpylä P J, Korpi J and Brandenburg A 2008 *Astron. Astrophys.* **491** 353
[17] Yousef T A, Heinemann T, Schekochihin A A, Kleeorin N, Rogachevskii I, Iskakov A B, Cowley S C and McWilliams J C 2008a *Phys. Rev. Lett* **100** 184501
[18] Yousef T A, Heinemann T, Rincon F, Schekochihin A A, Kleeorin N, Rogachevskii I, Cowley S C and McWilliams J C 2008b *Astron. Nachr.* **329** 737
[19] Käpylä P J and Brandenburg A 2009 *Astrophys. J.* **699** 1059
[20] Hughes D W and Proctor M R E 2009 *Phys. Rev. Lett.* **102** 044501
[21] Hughes D W and Proctor M R E 2013 *J. Fluid Mech.* **717** 395
[22] Heinemann T, McWilliams J C and Schekochihin A A 2012 *Phys. Rev. Lett.* **107** 255004
[23] Mitra D and Brandenburg A 2012 *Mon. Not. R. Astron. Soc.* **420** 2170
[24] Teed R J and Proctor M R E 2016 *Mon. Not. R. Astron. Soc.* **458 2885**
[25] Leprovost N and Kim E 2008 *Phys. Rev. Lett.* **100** 144502
[26] Leprovost N and Kim E 2009 *Astrophys. J.* **696** L125
[27] Leprovost N and Kim E 2008 *Phys. Rev. E* **78** 036319
[28] Courvoisier A and Kim E 2009 *Phys. Rev. E* **80** 046308
[29] Tobias S M and Cattaneo F 2013 *Nature* **497** 463
[30] Hollerbach R 2000 *Int. J. Numer. Meth. Fluids* **32** 773
[31] Kim E 2004 *Mod. Phys. Lett. B* **18** 1
[32] Livermore P W, Hughes D W and Tobias S M 2010 *Phys. Fluids* **22** 013002